Preformed portals facilitate dendritic cell entry into afferent lymphatic vessels

Holger Pflicke and Michael Sixt

Max Planck Institute of Biochemistry, Hofschneider Group Leukocyte Migration, 82152 Martinsried, Germany

Although both processes occur at similar rates, leukocyte extravasation from the blood circulation is well investigated, whereas intravasation into lymphatic vessels has hardly been studied. In contrast to a common assumption—that intra- and extravasation follow similar molecular principles—we previously showed that lymphatic entry of dendritic cells (DCs) does not require integrin-mediated adhesive interactions. In this study, we demonstrate that DC-entry is also independent of pericellular proteolysis, raising the question of whether lymphatic vessels offer preexisting entry routes. We find that the perilymphatic basement membrane of initial lymphatic vessels is discontinuous and therefore leaves gaps for entering cells. Using a newly developed in situ live cell imaging approach that allows us to dynamically visualize the cells and their extracellular environment, we demonstrate that DCs enter through these discontinuities, which are transiently mechanically dilated by the passaging cells. We further show that penetration of the underlying lymphatic endothelial layer occurs through flap valves lacking continuous intercellular junctions. Together, we demonstrate free cellular communication between interstitium and lymphatic lumen.

CORRESPONDENCE
Michael Sixt:
sixt@biochem.mpg.de

Abbreviations used: BM, basement membrane; bmDC, bone marrow–derived DC.

The interstitial space of the dermis maintains an open one-way communication with the lymphatic system. A constant interstitial flux drags serum components filtrated from the capillary bed toward the initial lymphatic vessels that are equipped with flap valves to allow entry but prevent exit of solutes and small particles (Swartz, 2001; Trzewik et al., 2001). Patrolling immune cells like lymphocytes (Debes et al., 2005) and DCs (Alvarez et al., 2008), but also hematopoietic stem cells (Massberg et al., 2007), follow the same principal route. Whereas fluid flux is driven by the periodic contractions of the lymphatic suction pump (Swartz, 2001), cells rely on autonomous action and crawl through the interstitium toward and into the initial lymphatic vessel. The major guidance cues for this migration are chemokines that are expressed by the lymphatic endothelium and sensed by hematopoietic cells (Alvarez et al., 2008). We recently showed that leukocytes crawl through the interstitium without specific integrin-mediated contacts with their environment. This mode of locomotion is driven by the protrusive forward flow of polymerizing actin and occasionally supported by actomyosin contractions of the rear end to squeeze the rigid nucleus through narrow spaces (Lämmermann et al., 2008). Such movement is facilitated by extreme plasticity of the cell body, which led to the morphological description "amoeboid" migration (Friedl et al., 2001). Integrin-independent movement is mainly limited to three-dimensional environments (Hawkins et al., 2009) with large pore size, but fails when the cells have to move along two-dimensional surfaces or penetrate dense or stiff barriers like basement membranes (BMs) or endothelial linings (Lämmermann et al., 2008). The crossing of the blood endothelium is a well-investigated example where leukocytes require a cascade of tightly controlled molecular interactions to dissolve and penetrate the junctional sealing of the cell layer (Butcher and Picker, 1996; Ley et al., 2007). Hence, we were surprised to find that DCs do not require integrin-mediated cell–cell and cell–matrix interactions to enter lymphatics of mouse dermis and wondered how the vessel architecture might support cellular entry.

Here, we demonstrate that lymphatics are covered by a BM, but that this BM is discontinuous especially in the initial lymphatics that

The Rockefeller University Press $30.00
J. Exp. Med. Vol. 206 No. 13 2925-2935
www.jem.org/cgi/doi/10.1084/jem.20091739

The Journal of Experimental Medicine

serve as entry sites for blood cells. We show that DCs enter the lymphatics by squeezing through these preformed pores and subsequent passage through the flap valves of the lymphatic endothelium that lack continuous junctions. Such entry via preformed routes is in line with our findings that proteases and integrins are dispensable for intravasation.

RESULTS AND DISCUSSION

Two modes of DC migration into lymphatic vessels

We used a novel in situ live cell imaging approach to follow DC migration in explanted ear sheets of mice. In these "crawl-in" assays, split ear sheets were fluorescently stained with antibodies against either laminin or collagen IV to visualize BMs in the dermis. The ear sheets were mounted onto the bottom of climatized migration chambers and subsequently fluorescently labeled mature bone marrow–derived DCs (bmDCs) or endogenous DCs were added. After a short incubation that allowed the DCs to infiltrate the dermis, the preparation was imaged with spinning disc confocal microscopy.

The BM staining allowed morphological identification of arteries, veins, associated nerves, fat cells, and lymphatic vessels. Initial lymphatic vessels were characterized by their blind endings and their large and irregular diameter (Baluk et al., 2007). DCs selectively and directionally approached and entered the lymphatic vessels and after 90–120 min, almost all DCs had entered the lumen (Fig. 1 A and Video 1). Quantification of crawl-in videos revealed two types of behavior once the cells reached the BM of the lymphatic vessel: some cells slowed close to the BM before they again accelerated in the lumen of the vessel, whereas others migrated straight into the lumen (Fig. 1 B and Video 1).

We reasoned that this pattern emerged because initially entering DCs might create a path that is then used by the DCs that follow. Path generation through BMs was mainly attributed to the MMP family of proteases (Rowe and Weiss, 2008). However, to additionally exclude effects by other proteases, we applied a previously described protease inhibitor cocktail that was shown to block any pericellular proteolytic activity in vitro and in vivo (Wolf et al., 2003). We tracked single-cell velocities of intravasating bmDCs and could neither detect reduced interstitial migration speeds nor hampered intravasation (Fig. 1, C and E). To control this approach, we quantified migration of bmDCs across an in vitro assembled BM: to this end, long-term cultured immortalized epithelial cells were lysed off of filters, revealing a tightly assembled BM (Furuyama and Mochitate, 2000 and not depicted). bmDCs were layered onto these BMs and transmigration was quantified after overnight exposure. In this setup, applying the protease inhibitor cocktail entirely inhibited transmigration (Fig. 1 D), which is in line with a study showing that epidermal DCs require MMPs to cross the epidermal BM (Ratzinger et al., 2002).

The finding that pericellular proteolysis was dispensable for lymphatic entry was consistent with our previous data that intravasation was also independent of integrins (Lämmermann et al., 2008) that restrict proteolytic activity to the site of potential invasion (Gimona et al., 2008). Intravasation was entirely dependent on directional sensing via CCR7, as CCR7-deficient DCs neither approached nor entered lymphatic vessels (Fig. S3 A), supporting previous findings that CCR7 is the key factor mediating intravasation (Förster et al., 1999; Ohl et al., 2004).

The perilymphatic BM is discontinuous

As the data strongly argued against active path generation by DCs, we investigated preformed anatomical entry routes as a second possible explanation for our initial observations. Hence, we investigated the structural features of the lymphatic BM of ear skin in more detail.

In thin-section histology, the lymphatic BM is not easily detectable (Petrova et al., 2004; Vainionpää et al., 2007). When we performed whole-mount immunohistology of ear skin, we obtained a clear signal around LYVE-1–positive lymphatic vessels for all essential BM components (Fig. 2); collagen IV, laminins, perlecan, and nidogen formed a sheet around the blind-ending initial lymphatic vessels. Co-localization of all components was perfect in this area, although nidogen was also detectable in patches within the dermis (Fig. 2 B), which is in line with its expression by dermal fibroblasts (Breitkreutz et al., 2004). Together with immunoelectronmicroscopy studies that showed an electron-dense structure associated with type IV collagens and laminin at the outline of lymphatics (Sauter et al., 1998), this argues for a regularly assembled BM at the abluminal lymphatic surface.

In comparison to the continuous appearance of blood capillary and fat cell BMs, the lymphatic BM showed a lower fluorescence signal and discontinuities (Fig. 2 A). Higher magnification views and three-dimensional reconstructions revealed that the discontinuities were not sites of low expression of single BM components as shown for the perivenular BM (Wang et al., 2006), but rather areas completely devoid of any of the analyzed BM components (Fig. 2 B).

Lymphatic vessels can be subdivided in the blind ending initial lymphatic capillaries and the draining collector vessels. Collectors are characterized by no LYVE-1, but maintained gp38 expression (Mäkinen et al., 2005). Co-staining of gp38, LYVE-1, and collagen IV revealed that in contrast to lymphatic capillaries the BM of collectors is not perforated (Fig. 3, A and B). We morphometrically quantified the perforated surface area in relation to the total lymph vessel surface and found that the perforated area was <5% in collectors, whereas in lymphatic capillaries it accounted for up to 30% of the total vessel area (Fig. 3 C). Using the identical morphometric intensity thresholding for blood vessels, we could not detect any perforated areas in the same tissue samples. The "low expression sites" that serve as exit sites for granulocytes extravasating via postcapillary venule BMs (Wang et al., 2006) could only be detected when intensity thresholds were reduced, confirming that these areas are indeed regions of low BM molecule deposition rather than true perforations as they are found in the lymphatics (unpublished data).

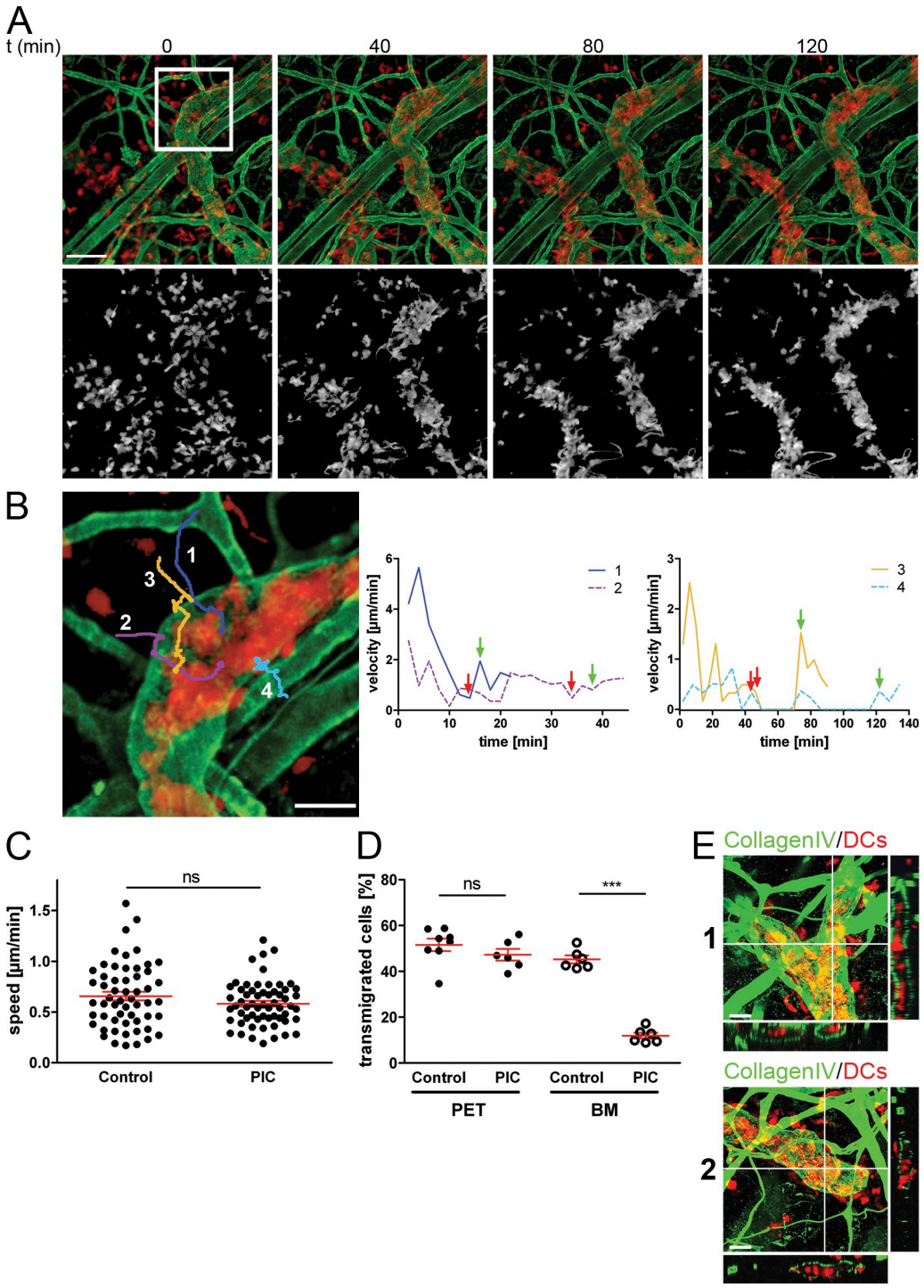

Figure 1. DCs display two types of migration modes into lymphatic vessels. (A) Spinning disc confocal images (maximum projection of z-stack, 22 planes, 0.5 µm distance) of labeled DCs (red) migrating into lymphatic vessels (BM stained for laminin, green) over time. See also Video 1. Bar, 50 µm. (B) Enlargement of inset in (A) representatively showing tracks of four different DCs. Bar, 20 µm. On the right of the panel instantaneous velocities of the DCs (tracks 1–4) are plotted over time. Arrival at the lymphatic vessel BM is marked by a red and appearance in the vessel lumen by a green arrow. (C) Average migration velocities in the presence of DMSO (control) or protease inhibitor cocktail (PIC). Control: 5 independent preparations, 56 cells tracked. PIC: 7 independent preparations, 61 cells tracked. Error bars show the mean ± SE of mean (SEM). ns, not significant. (D) DC migration across plain transwell (PET) vs. transwell carrying an in vitro assembled BM (BM) in the presence of DMSO (control) or PIC. One representative of two independent experiments. Each dot represents a single transwell used in the experiment. Error bars show mean ± SEM. ns, not significant. ***, $P < 0.0001$ (E) Confocal images of whole-mount ear skin 2 h after addition of exogenously labeled bmDCs. DCs were incubated before crawl-in assay with either DMSO (1) or protease inhibitor (2). Bar, 20 µm. Images are representatives of one of at least five independently performed crawl-in assays.

Reasons for the fragility of this BM might be twofold: first, lymphatic endothelial cells express low levels of RNA coding for BM molecules (Podgrabinska et al., 2002; Hirakawa et al., 2003). Second, the initial lymphatics lack pericytes, which are an abundant source of BM constituents (Petrova et al., 2004; Hallmann et al., 2005). Interestingly, it was shown that in *foxc2* knockout mice, which is the mouse model for the human disease lymphedema distichiasis, initial lymphatics are aberrantly invested by pericytes (Petrova et al., 2004) and that this leads to the enhanced deposition of BM components in lymphatic capillaries. This suggests that either pericytes contribute directly to the BM or indirectly influence the matrix production or deposition of the lymphatic endothelium.

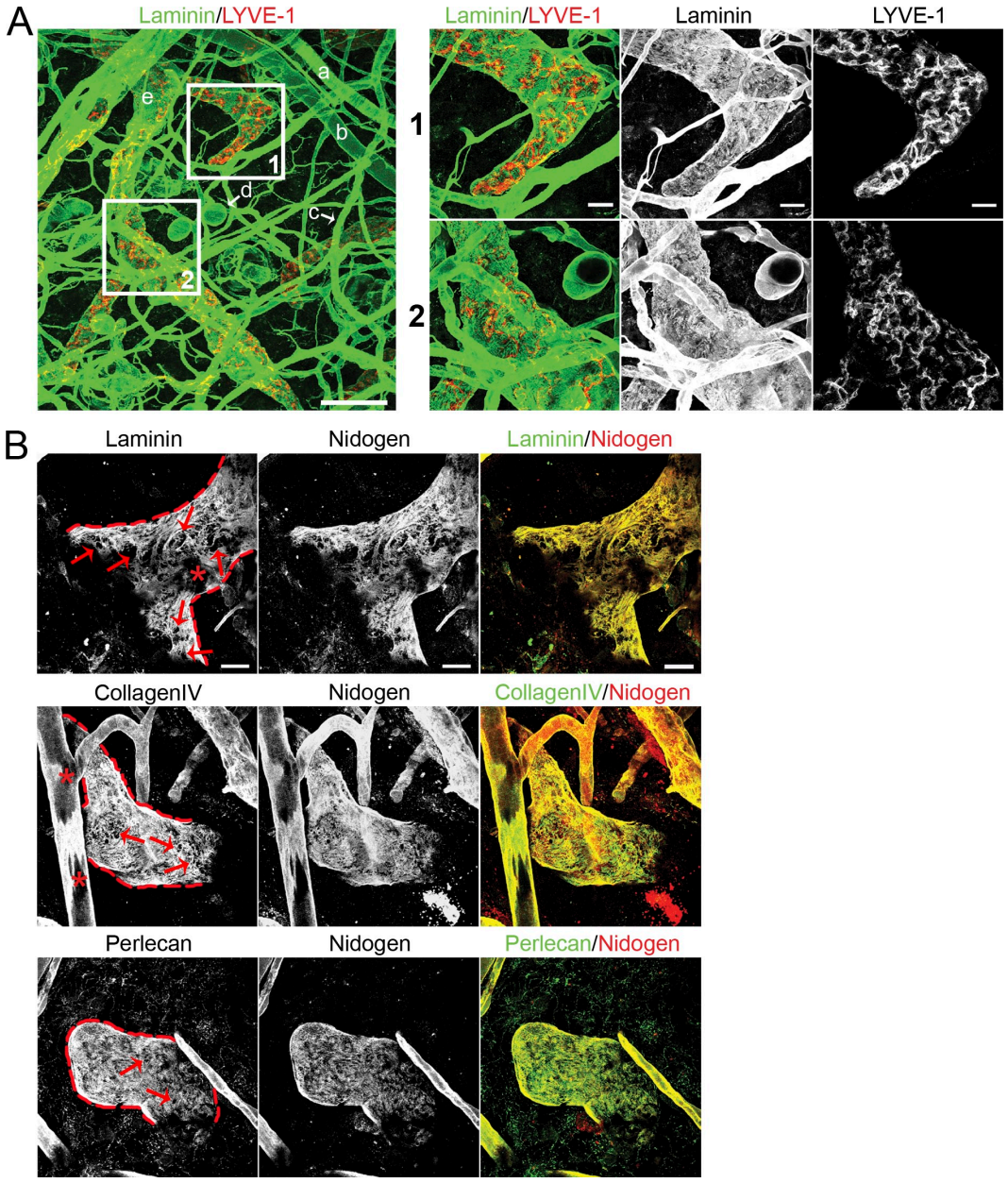

Figure 2. Discontinuous expression of BM components on initial lymphatic vessels. (A) Confocal images of whole-mount ear skin preparations. BMs were identified by staining for laminin (green) and lymphatic vessels were identified by staining for LYVE-1 (red), respectively. The following tissue structures can be distinguished: a, arteriole; b, vein; c, capillary; d, fat cell; e, lymphatic vessel. Bar, 100 µm. Insets 1 and 2 show higher magnification pictures of respective areas on initial lymphatics. Bar, 20 µm. (B) Co-localization of major BM components on initial lymphatics. Lymphatic vessel edges are outlined red. Note the clear contours of BM perforations (arrows). Asterisks show areas on a lymphatic vessel (top row) and blood vessel (middle row), which do not represent perforations but rather tangential sections of the vessels caused by the limited z volume. Bar, 20 µm. Images are representatives of one of at least 11 different tissues investigated.

DCs traverse the lymphatic BM via discontinuities

The discovery of BM discontinuities in lymphatic capillaries raised the possibility that these sites may be used as entry portals by approaching DCs. To address this possibility, we recorded high-magnification time-lapse z-series of bmDCs and lymph vessel BM.

Strikingly, in all cases where we could observe DCs entering the lymphatic lumen, the cells used preexisting discontinuities as entry sites. Approaching DCs inserted a protrusion into the BM perforation, and subsequently the cell body was propelled across the BM (Fig. 4, A and B, Fig. S1, and Videos S2–S6). Although it would be interesting to know if DCs are able to penetrate the unperforated BMs of collector vessels, we could never observe bmDCs approaching or entering at these sites (Fig. S4). This was despite the more superficial localization of collectors in our preparations, which is caused by the fact that collectors are buried deeper in the ear dermis than initial lymphatic vessels.

BM discontinuities are extended during cellular passage

The finding that BM penetration apparently requires neither biochemical remodelling nor specific adhesion prompted us to investigate possible extension forces imposed by the DCs squeezing through BM perforations. We therefore analyzed the distribution of BM immunostainings during cellular passage. We focused on intravasation events that involved significant extension of BM perforations and found that fluorescence intensity at the lateral margins of the entry hole increased upon passage (Fig. 4 C). This indicates that the BM is not degraded, but rather pushed aside by hydrostatic forces

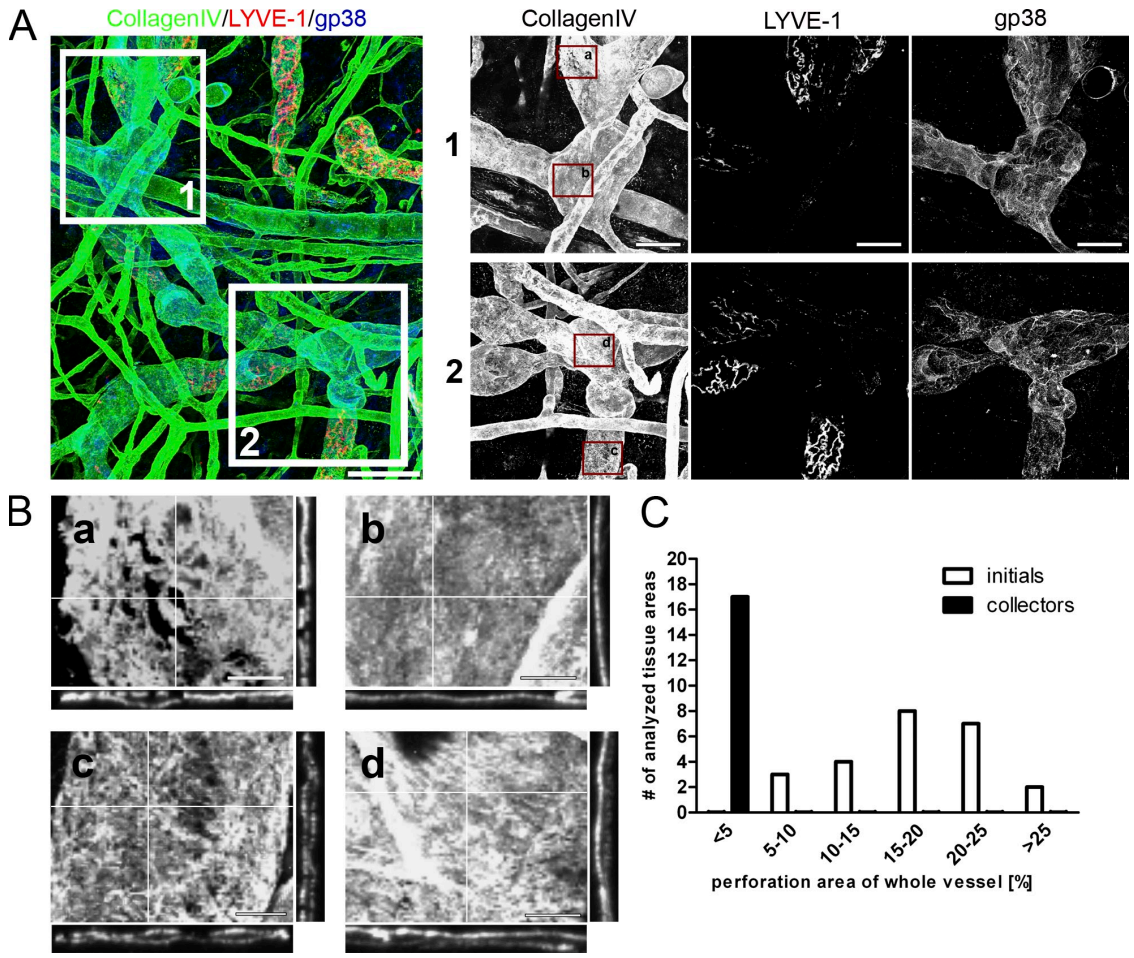

Figure 3. Collecting lymphatic vessels show continuous BM. (A) Confocal images of whole-mount ear skin preparations. BMs were identified by staining for collagen IV (green) and initial lymphatic vessels were identified by staining for LYVE-1 (red) and gp38 (blue). Collectors were identified by the lack of a LYVE-1 staining, but preserved gp38 staining. Bar, 100 µm. Insets 1 and 2 show higher magnification images of respective areas on collecting lymphatics. Bar, 50 µm. (B) Enlargements of insets in A demonstrating the discontinuous BM assembly on initial lymphatics in a and c in stark contrast to BM assembly on collector lymphatic vessels (b and d). Note the even distribution of collagen IV in b and d orthogonal plane views compared with a and c. Bar, 20 µm. (C) Quantification of perforation area in relation to total lymphatic vessel area for initial and collector lymphatics. Every single vessel area analyzed was grouped according to the fraction of the BM perforation area of the whole vessel area analyzed. Images are representatives of one of at least nine different tissues investigated. For the quantification in C, 24 areas in 11 different tissues were analyzed for initial lymphatic vessels and 17 areas in 9 different tissues were analyzed for collector lymphatic vessels.

exerted by the DC (Fig. S2 and Videos S4–S6). Such deformation is reminiscent of findings with amoeboid tumor cells migrating through collagen scaffolds (Wyckoff et al., 2006). To consolidate the aforementioned observation, we morphometrically quantified the number of perforations before and after passage of large quantities of bmDCs. Using identical thresholding parameters, the number of perforations per area was not altered 90 min after addition of the cells, excluding de novo generation of perforations by migrating bmDCs (Fig. 5 A). To ensure that the migration pattern of bmDCs

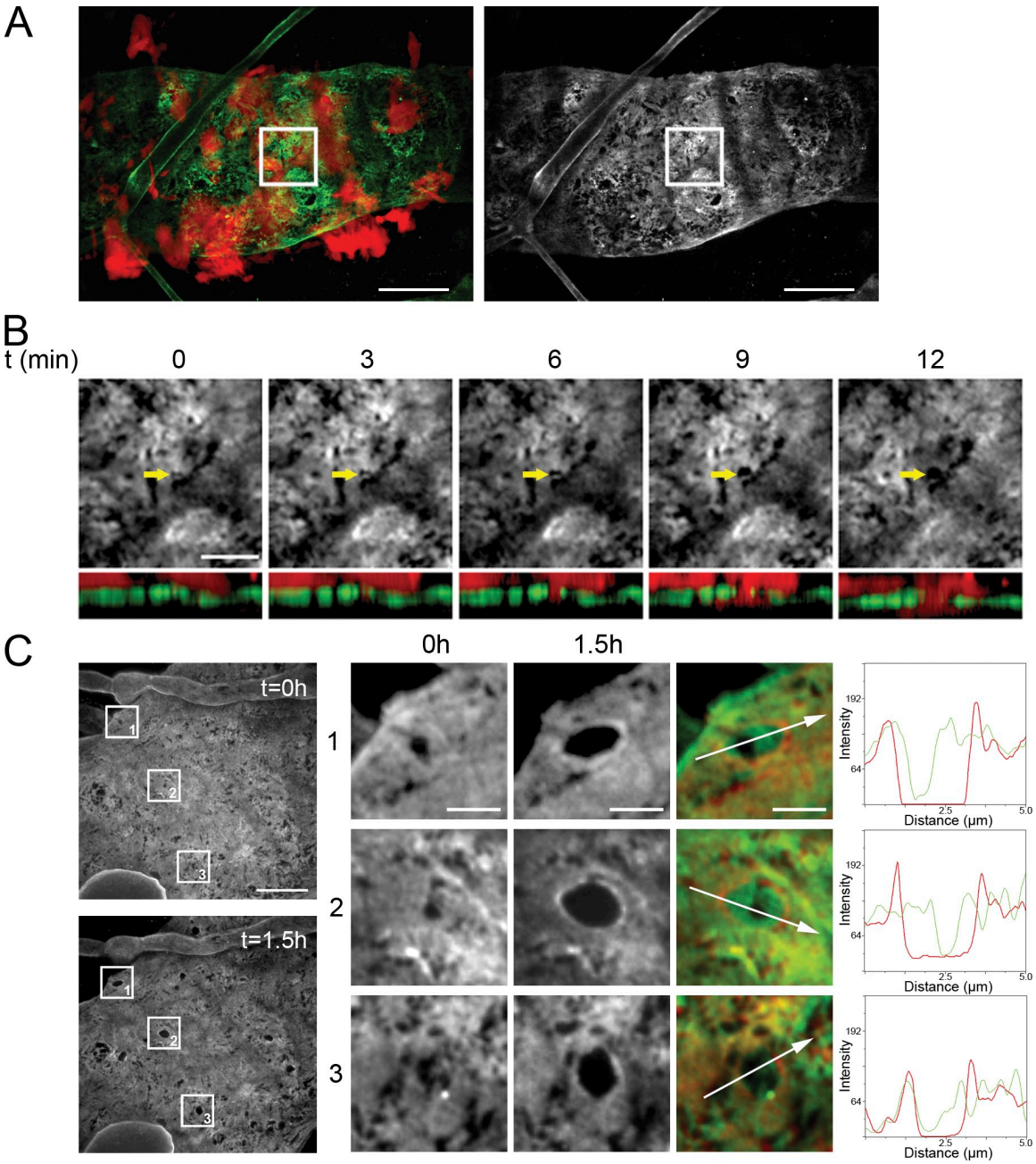

Figure 4. DCs dilate BM perforations. (A) Spinning disk confocal images (maximum projection of z-stack, 10 planes, 0.5 µm distance) of DCs (red) in close vicinity of an initial lymphatic vessel (BM staining: collagen IV, green; blood capillary also visible). Bar, 20 µm. (B) Inset of A showing the initial events of a single DC (red) entering the vessel lumen via a preexisting perforation (arrow; maximum projection of z-stack, 5 planes, 0.5 µm distance). Top row shows the top view onto vessel BM (collagen IV), the bottom row the corresponding sectional XZ-view (BM green; DC red). Bar, 5 µm. (C) Representative spinning disk confocal images of an initial lymphatic vessel showing the enlargement of perforations (BM staining: collagen IV) over a period of 1.5 h. Bar, 10 µm. Enlargements of insets 1–3 are shown on the right. Overlay images show perforation size at $t = 0$ h (green) and $t = 1.5$ h (red). Bar, 2 µm. A histogram plot of the line section across the perforation shows fluorescence intensity of collagen IV at $t = 0$ h in green and at $t = 1.5$ h in red. Images are representatives of one of at least nine independently performed crawl-in assays.

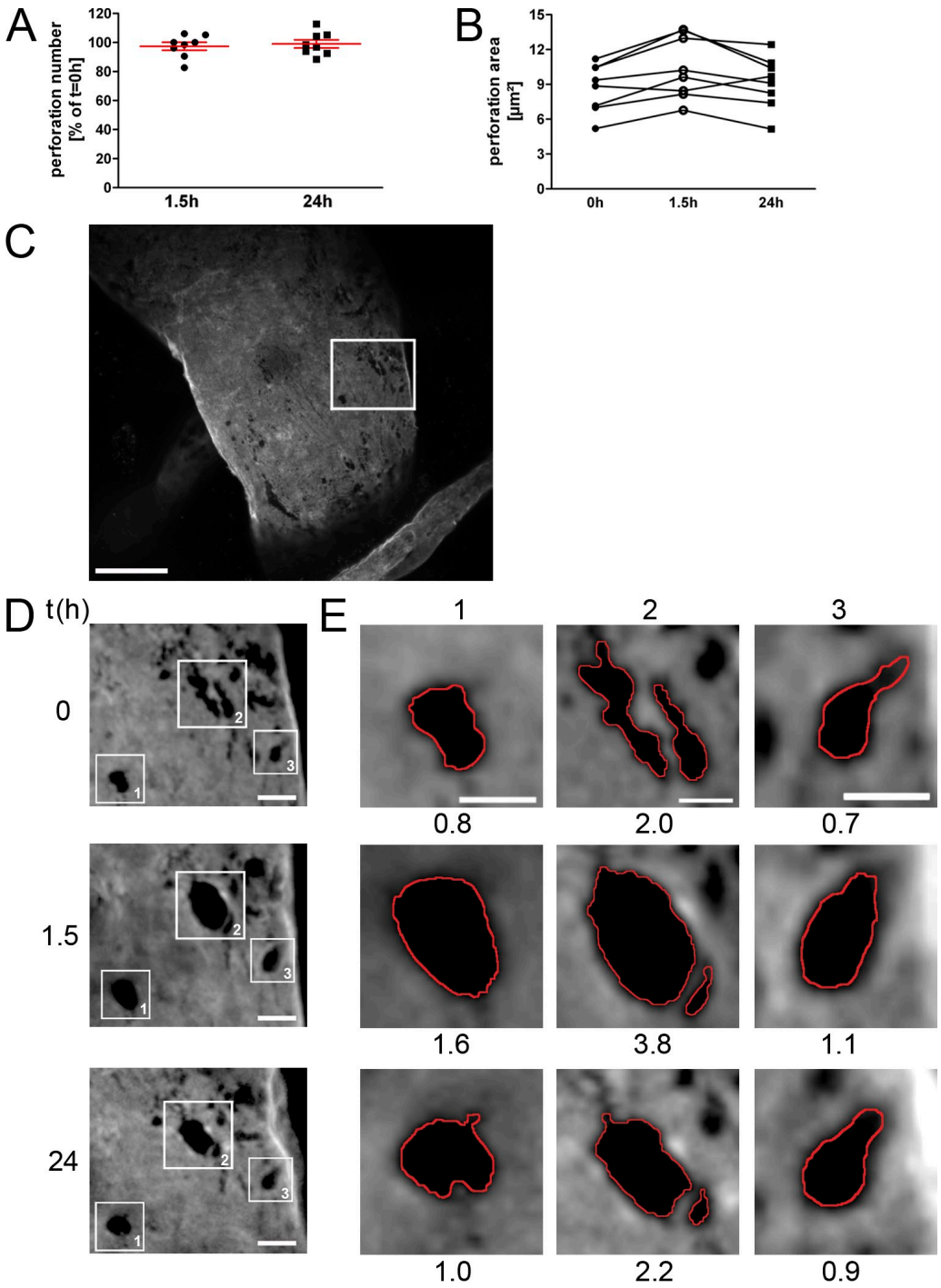

Figure 5. BM perforation dilation is a transient event. (A) Quantification of perforation number on initial lymphatic vessels in crawl-in assays at time points $t = 1.5$ h and $t = 24$ h. Six different tissues (up to two areas per tissue) were imaged at the indicated time points and analyzed morphometrically. Perforation number and area at $t = 0$ h was set to 100%. Each dot represents one analyzed area. Error bars show mean ± SEM (B) Quantification of perforation area on initial lymphatic vessels in crawl-in assays at time points $t = 0$ h, $t = 1.5$ h, and $t = 24$ h. Six different tissues (up to two areas per tissue) were imaged at the indicated time points and analyzed morphometrically. (C) Initial lymphatic vessel (BM staining for collagen IV; blood capillary also visible in bottom right corner) visualized using a spinning disk confocal microscope (maximum projection of z-stack, 4 planes, 0.5 µm distance). Bar, 20 µm. (D) Enlargement of inset in C showing perforation size at $t = 0$ h, $t = 1.5$ h, and after 24 h of addition of DCs to ear explant. Bar, 10 µm. (E) Representative analysis of the perforation area after migration of DCs into the lumen of an initial lymphatic vessel. During the course of 24 h, BM perforations get dilated (1.5 h) and relax again (24 h). Enlargement of inset 1–3 in D showing perforation size at $t = 0$ h, $t = 1.5$ h, and after 24 h. Numbers below each image denote perforation area (red line) in square micrometers. Bars, 2 µm. Images are representatives of one of at least three independently performed crawl-in assays.

does not differ from that of endogenous DCs we used DCs that previously emigrated from ear tissue. In crawl-in assays these cells also entered via preexisting perforations (Fig. S1), demonstrating that this mode of intravasation is universal for DCs.

The homeostatic dermis experiences a constant steady-state flux of DCs and other hematopoietic cells, raising the possibility that these cells create the perforations. However, when we examined dermis of *CCR7*$^{-/-}$ mice, where steady-state migration of most hematopoietic cells, including DCs, is abolished (Ohl et al., 2004), we found the same surface area perforated (Fig. S3 B). This suggests that perforations are an intrinsic property of lymphatic capillaries rather than the result of continuously passaging cells.

Assuming a certain elasticity of the BM, deformations could be transient, as the locally compressed BM might relax and reextend after the cell has left the gap. To address if the BM reverts to its original state after DCs entered the vessel lumen, samples were left under assay conditions for 24 h and BM discontinuities were measured. Quantification showed that BMs partially relax after intravasation (Fig. 5, B–E), adding to our previous evidence that proteolytic modification of the BM is not decisive for intravasation.

The finding that even small preexisting openings can be invaded by a cellular protrusion means that the lymphatic BM biophysically rather resembles a 3D scaffold than a sheet-like barrier. Once the cell's leading edge is inserted into a perforation, it can swell through actin polymerization and form an initial mechanical anchor. Subsequent trailing edge contraction can squeeze cytoplasm and the rigid nucleus through the gap, as we have shown for DCs migrating in three-dimensional collagen gels (Lämmermann et al., 2008). Such behavior does not rely on transmembrane force coupling via integrins and can generate sufficient hydrostatic pressure to extend the pore to a diameter sufficient to propel the nucleus (Wolf et al., 2007; Lämmermann et al., 2008). Our observation that the BM becomes compressed at the pore margins and relaxes after passage clearly argues for such a biophysical rather than a proteolytic scenario.

DCs pass through endothelial flap valves

The lymphatic BM is the initial barrier for intravasating DCs, and directly after their passage DCs face the lymphatic endothelium. Endothelial cells of the initial lymphatics are interconnected by specialized junctional complexes that contain components similar to blood vessel endothelium but are assembled in entirely different structures. Instead of the continuous zipperlike distribution found in blood endothelium, lymphatics show a buttonlike distribution of junctional components. These buttons likely form the "hinges" of the flap valves. The spacing between the buttons was shown to be 2–3 µm (Baluk et al., 2007), which might allow cellular passage without dissolution of junctions.

To test this assumption, we stained ear sheets with LYVE-1 antibody and performed crawl-in assays. As described by Baluk et al. (2007), LYVE-1 outlined single endothelial cells revealing their oak leaf structure with the peripheral lobes representing the flexible areas that are interconnected by buttons at their base. When the LYVE-1 pattern was imaged in ears without exogenously added DCs, the endothelial outlines remained static (unpublished data). During bmDC intravasation, the peripheral lobes of endothelial cells were locally deformed (Fig. 6, A and B; Videos S7 and S8) and analysis of z-time series supported a model where flaps bend into the lymphatic lumen during DC passage (Fig. 6, C and D) while the button-junctions at the flap-base remain in position. The entry via gaps between button junctions also resembles ultrastructural findings where metastasizing tumor cells were demonstrated to passage through "intercellular channels" between the lymphatic endothelial cells (Azzali, 2007).

Our finding that DCs can cross the lymphatic vessel within a few minutes is in contrast to in vitro studies where DCs took 3–6 h to cross a monolayer of a lymphatic endothelial cell line (Johnson et al., 2006). We explain these differences by the fact that lymphatic monolayers do not assemble button junctions, but rather the zipperlike junctions of blood endothelium or lymphatic collector vessels (Kriehuber et al., 2001). Rapid intravasation via preformed portals is reminiscent of lymphocytes passaging through portals within the medullary sinus of the lymph node (Wei et al., 2005), with the exception that we never observed DCs reexiting from the lymph vessel. Preformed portals further explain our findings that integrin-deficient cells intravasate normally, which again corresponds well with the fact that homeostatic lymphatics do not express the cellular integrin ligands ICAM-1 and VCAM-1 (Johnson et al., 2006; Teoh et al., 2009). This situation might change in the inflammatory state, where ICAM-1 and VCAM-1 are strongly induced on the lymphatics and adhesion gains functional importance (Johnson et al., 2006; Ledgerwood et al., 2008).

In conclusion, we find that a physical barrier is largely lacking at the level of the homeostatic lymphatic endothelium, and therefore informational cues like chemokines are the decisive factors guiding the cells into the lymphatics. These findings support the concept of an open cellular communication between interstitium and draining lymph node, and suggest that only the lymph node serves as the physiological filtration station (Lämmermann and Sixt, 2008).

MATERIALS AND METHODS

Animals. C57BL/6 mice were kept in a conventional animal facility at the Max Planck Institute of Biochemistry. Mouse breeding and experimental procedures were approved by the Regierung von Oberbayern.

Generation of DCs. DCs were generated from flushed bone marrow suspension as described previously (Lutz et al., 1999). At day 9–12 of culture, 200 ng/ml LPS (Sigma-Aldrich; *E. coli* 0127:B8) was added overnight. Endogenous DCs were isolated by floating ventral sheets on culture medium (RPMI 1640 supplemented with 10% fetal calf serum, 1% glutamine, and 1% penicillin/streptomycin) for 72 h and pooling emigrated DCs. For imaging, cells were fluorescently labeled with Tetra-Methylrhodamine (Invitrogen).

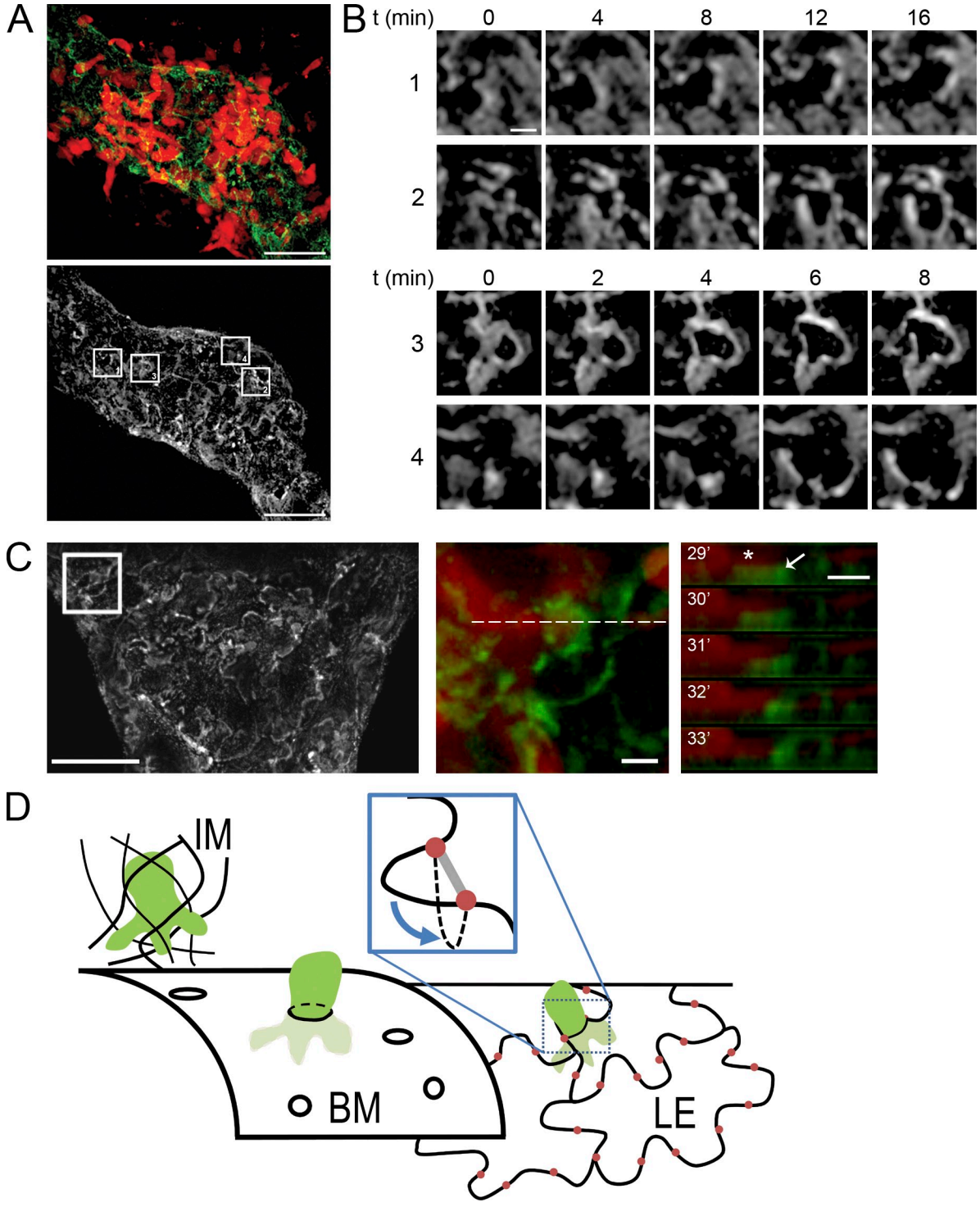

Figure 6. DCs enter vessel lumen via endothelial flap valves. (A, top) DCs (red) entering an initial lymphatic vessel stained with LYVE-1 (green), which highlights the outline of lymphatic endothelial cells. (bottom) LYVE-1 staining only; boxes highlight the areas displayed in B. Bars, 20 µm. (B) Time series of highlighted areas showing movement of endothelial cell edges upon entry of DCs. Bar, 2 µm. (C) LYVE-1 staining of an initial lymphatic vessel. Bar, 20 µm. (middle) Highlighted area where a DC enters. (right) The z-projected time series of the dotted line shown in the middle panel. Note the DC protrusion (red, asterisk) adjacent to the LYVE-1–positive structure that bends downward (into the vessel lumen). Bars, 2 µm. Images are representatives of one of eight independent experiments. (D) Schematic summarizing the findings. DCs (green) arrive via the interstitial matrix (IM) and encounter the porous BM of the initial lymphatic vessel. They enter by squeezing through the pores and subsequently encounter the lymphatic endothelial layer (LE). The oak leaf–shaped lymphatic endothelial cells are interconnected by junctional complexes organized as buttons (red) at the base of flexible lobes. DCs enter the endothelial layer without opening the junctions by pushing the flap valves into the vessel lumen (inset).

Whole-mount ear skin immunohistology. Mice were sacrificed, and their ears were removed and separated into dorsal and ventral sheets. Cartilage-free ventral ear sheets were fixed with 1% paraformaldehyde, immersed in 0.2% Triton X-100, washed with PBS, blocked with 1% BSA (PAA Laboratories), and incubated with primary antibodies diluted in PBS 1% BSA over night at 4°C. The antibodies used were as follows: rabbit anti-collagen IV (1119+; T. Sasaki, Max Planck Institute of Biochemistry, Martinsried, Germany); rabbit anti-laminin (L9393; Sigma-Aldrich), rabbit anti-perlecan domain V (1056+; R. Timpl, Max Planck Institute of Biochemistry; Brown et al., 1997); rat anti-nidogen (ELM1; Millipore); rat polyclonal anti-LYVE-1 antibody (clone 223322; R&D Systems); and hamster anti-gp38 (clone 8.1.1; Farr et al., 1992). Secondary antibodies were conjugated with cy3, cy5 (Jackson Immunoresearch Laboratories), Alexa Fluor 488, and Alexa Fluor 647 (Invitrogen). Images were acquired with a confocal laser-scanning microscope (Leica DMIRE2; objectives HC PL APO 20×/0.70, HCX PL APO 63×/1.4-0.60, and HCX PL APO 100×/1.4-0.70), and image analysis was performed using Metamorph software (Molecular Devices).

Image analysis. Confocal z-stacks of lymph vessel walls were projected using the Metamorph maximum projection tool. Videos were processed using background subtraction and low-pass filter. To enhance Tetra-Methylrhodamine, staining of DCs γ value was set to two in some cases. Perforation areas were quantified using manual thresholding, and subsequent measurement with the morphometric analysis tool of Metamorph.

In vitro transmigration assay. BMs were assembled in vitro using a modified protocol of Furuyama and Mochitate (Furuyama and Mochitate, 2000). In brief, SV40T2 immortalized alveolar type II epithelial cells (gift from A. Clement, Hopital Trousseau, Paris; Clement et al., 1991) were cultured in Transwell dishes (BD) supplemented with Matrigel (BD) for 2–3 wk and BMs were denuded using 0.25 M ammonium hydroxide and repeated washing with PBS.

Mature DCs were preincubated for 1 h at 37°C with protease inhibitor cocktail (Wolf et al., 2003) consisting of 50 µM GM6001 (Merck Chemicals); 20 µM E-64 (Sigma-Aldrich); 20 µM pepstatin A (Sigma-Aldrich); 2 µM leupeptin (Sigma-Aldrich); aprotinin (Chemicon); or carrier control. 10^5 cells in 200 µl were added to the upper compartment of 8 µm pore size Transwells. 1 µg/ml CCL21 (R&D Systems) was added to the lower compartments, and after overnight incubation transmigrated DCs were counted with a hemocytometer.

Ex vivo crawl-in assay and time-lapse video microscopy. Unfixed ventral ear sheets were immunostained and mounted on custom-built migration chambers with the dermal surface exposed. TAMRA-labeled DCs in culture medium were added onto the dermis and incubated for 5–15 min at 37°C, 5% CO_2. After removing noninfiltrated DCs, ear sheets were imaged in a climatized (37°C, 5% CO_2) chamber with a spinning-disk confocal microscope (Axio Observer Z1; Carl Zeiss, Inc.) equipped with EC Plan-Neofluar 10×/0.30, EC Plan-Neofluar 20×/0.5, and Plan-Apochromat 40×/0.95 objectives, an Optovar (1.6×), and a CoolSNAP HQ^2 CCD camera (Visitron Systems).

Cell tracking. Cells were tracked using the "Manual Tracking Plug-in" of ImageJ (http://rsbweb.nih.gov/ij/) and analyzed with the "Chemotaxis and Migration Tool Plug-in" (http://www.ibidi.de/applications/ap_chemo.html).

Statistical analysis. Student's *t* tests were performed after data were confirmed to fulfill the criteria of normal distribution, and P values were calculated using the GraphPadPlus software.

Online supplemental material. Fig. S1 shows intravasation of endogenous DCs. Fig. S2 provides overview images of the Videos S4–S6. Fig. S3 shows BMs in CCR7-deficient tissue, as well as migration of CCR7-deficient DCs in crawl-in assays. Fig. S4 documents the lack of intravasation into lymphatic collectors. Video S1 shows a low-magnification view of lymphatic intravasation. Videos S2–S6 show DCs invading the lymphatic BM and Videos S7 and S8 show DCs interacting with the lymphatic endothelium. Online supplemental material is available at http://www.jem.org/cgi/content/full/jem.20091739/DC1.

We thank Sylvia Cremer and all members of the Sixt laboratory for discussions and critical reading of the manuscript and Reinhard Fässler for continuous support.

This work was funded by the Peter Hans Hofschneider Foundation for Experimental Biomedicine, the German Research Foundation, and the Max Planck Society.

The authors declare that they have no conflicting financial interests.

Submitted: 10 August 2009
Accepted: 4 November 2009

REFERENCES

Alvarez, D., E.H. Vollmann, and U.H. von Andrian. 2008. Mechanisms and consequences of dendritic cell migration. *Immunity*. 29:325–342. doi:10.1016/j.immuni.2008.08.006

Azzali, G. 2007. Tumor cell transendothelial passage in the absorbing lymphatic vessel of transgenic adenocarcinoma mouse prostate. *Am. J. Pathol.* 170:334–346. doi:10.2353/ajpath.2007.060447

Baluk, P., J. Fuxe, H. Hashizume, T. Romano, E. Lashnits, S. Butz, D. Vestweber, M. Corada, C. Molendini, E. Dejana, and D.M. McDonald. 2007. Functionally specialized junctions between endothelial cells of lymphatic vessels. *J. Exp. Med.* 204:2349–2362. doi:10.1084/jem.20062596

Breitkreutz, D., N. Mirancea, C. Schmidt, R. Beck, U. Werner, H.J. Stark, M. Gerl, and N.E. Fusenig. 2004. Inhibition of basement membrane formation by a nidogen-binding laminin gamma1-chain fragment in human skin-organotypic cocultures. *J. Cell Sci.* 117:2611–2622. doi:10.1242/jcs.01127

Brown, J.C., T. Sasaki, W. Göhring, Y. Yamada, and R. Timpl. 1997. The C-terminal domain V of perlecan promotes beta1 integrin-mediated cell adhesion, binds heparin, nidogen and fibulin-2 and can be modified by glycosaminoglycans. *Eur. J. Biochem.* 250:39–46. doi:10.1111/j.1432-1033.1997.t01-1-00039.x

Butcher, E.C., and L.J. Picker. 1996. Lymphocyte homing and homeostasis. *Science*. 272:60–66. doi:10.1126/science.272.5258.60

Clement, A., M.P. Steele, J.S. Brody, and N. Riedel. 1991. SV40T-immortalized lung alveolar epithelial cells display post-transcriptional regulation of proliferation-related genes. *Exp. Cell Res.* 196:198–205. doi:10.1016/0014-4827(91)90251-O

Debes, G.F., C.N. Arnold, A.J. Young, S. Krautwald, M. Lipp, J.B. Hay, and E.C. Butcher. 2005. Chemokine receptor CCR7 required for T lymphocyte exit from peripheral tissues. *Nat. Immunol.* 6:889–894. doi:10.1038/ni1238

Farr, A., A. Nelson, and S. Hosier. 1992. Characterization of an antigenic determinant preferentially expressed by type I epithelial cells in the murine thymus. *J. Histochem. Cytochem.* 40:651–664.

Förster, R., A. Schubel, D. Breitfeld, E. Kremmer, I. Renner-Müller, E. Wolf, and M. Lipp. 1999. CCR7 coordinates the primary immune response by establishing functional microenvironments in secondary lymphoid organs. *Cell*. 99:23–33. doi:10.1016/S0092-8674(00)80059-8

Friedl, P., S. Borgmann, and E.B. Bröcker. 2001. Amoeboid leukocyte crawling through extracellular matrix: lessons from the Dictyostelium paradigm of cell movement. *J. Leukoc. Biol.* 70:491–509.

Furuyama, A., and K. Mochitate. 2000. Assembly of the exogenous extracellular matrix during basement membrane formation by alveolar epithelial cells in vitro. *J. Cell Sci.* 113:859–868.

Gimona, M., R. Buccione, S.A. Courtneidge, and S. Linder. 2008. Assembly and biological role of podosomes and invadopodia. *Curr. Opin. Cell Biol.* 20:235–241. doi:10.1016/j.ceb.2008.01.005

Hallmann, R., N. Horn, M. Selg, O. Wendler, F. Pausch, and L.M. Sorokin. 2005. Expression and function of laminins in the embryonic and mature vasculature. *Physiol. Rev.* 85:979–1000. doi:10.1152/physrev.00014.2004

Hawkins, R.J., M. Piel, G. Faure-Andre, A.M. Lennon-Dumenil, J.F. Joanny, J. Prost, and R. Voituriez. 2009. Pushing off the walls: a mechanism of cell motility in confinement. *Phys. Rev. Lett.* 102:058103. doi:10.1103/PhysRevLett.102.058103

Hirakawa, S., Y.K. Hong, N. Harvey, V. Schacht, K. Matsuda, T. Libermann, and M. Detmar. 2003. Identification of vascular lineage-specific genes by transcriptional profiling of isolated blood vascular and lymphatic endothelial cells. *Am. J. Pathol.* 162:575–586.

Johnson, L.A., S. Clasper, A.P. Holt, P.F. Lalor, D. Baban, and D.G. Jackson. 2006. An inflammation-induced mechanism for leukocyte transmigration across lymphatic vessel endothelium. *J. Exp. Med.* 203:2763–2777. doi:10.1084/jem.20051759

Kriehuber, E., S. Breiteneder-Geleff, M. Groeger, A. Soleiman, S.F. Schoppmann, G. Stingl, D. Kerjaschki, and D. Maurer. 2001. Isolation and characterization of dermal lymphatic and blood endothelial cells reveal stable and functionally specialized cell lineages. *J. Exp. Med.* 194:797–808. doi:10.1084/jem.194.6.797

Lämmermann, T., and M. Sixt. 2008. The microanatomy of T-cell responses. *Immunol. Rev.* 221:26–43. doi:10.1111/j.1600-065X.2008.00592.x

Lämmermann, T., B.L. Bader, S.J. Monkley, T. Worbs, R. Wedlich-Söldner, K. Hirsch, M. Keller, R. Förster, D.R. Critchley, R. Fässler, and M. Sixt. 2008. Rapid leukocyte migration by integrin-independent flowing and squeezing. *Nature.* 453:51–55. doi:10.1038/nature06887

Ledgerwood, L.G., G. Lal, N. Zhang, A. Garin, S.J. Esses, F. Ginhoux, M. Merad, H. Peche, S.A. Lira, Y. Ding, et al. 2008. The sphingosine 1-phosphate receptor 1 causes tissue retention by inhibiting the entry of peripheral tissue T lymphocytes into afferent lymphatics. *Nat. Immunol.* 9:42–53. doi:10.1038/ni1534

Ley, K., C. Laudanna, M.I. Cybulsky, and S. Nourshargh. 2007. Getting to the site of inflammation: the leukocyte adhesion cascade updated. *Nat. Rev. Immunol.* 7:678–689. doi:10.1038/nri2156

Lutz, M.B., N. Kukutsch, A.L. Ogilvie, S. Rössner, F. Koch, N. Romani, and G. Schuler. 1999. An advanced culture method for generating large quantities of highly pure dendritic cells from mouse bone marrow. *J. Immunol. Methods.* 223:77–92. doi:10.1016/S0022-1759(98)00204-X

Mäkinen, T., R.H. Adams, J. Bailey, Q. Lu, A. Ziemiecki, K. Alitalo, R. Klein, and G.A. Wilkinson. 2005. PDZ interaction site in ephrinB2 is required for the remodeling of lymphatic vasculature. *Genes Dev.* 19:397–410. doi:10.1101/gad.330105

Massberg, S., P. Schaerli, I. Knezevic-Maramica, M. Köllnberger, N. Tubo, E.A. Moseman, I.V. Huff, T. Junt, A.J. Wagers, I.B. Mazo, and U.H. von Andrian. 2007. Immunosurveillance by hematopoietic progenitor cells trafficking through blood, lymph, and peripheral tissues. *Cell.* 131:994–1008. doi:10.1016/j.cell.2007.09.047

Ohl, L., M. Mohaupt, N. Czeloth, G. Hintzen, Z. Kiafard, J. Zwirner, T. Blankenstein, G. Henning, and R. Förster. 2004. CCR7 governs skin dendritic cell migration under inflammatory and steady-state conditions. *Immunity.* 21:279–288. doi:10.1016/j.immuni.2004.06.014

Petrova, T.V., T. Karpanen, C. Norrmén, R. Mellor, T. Tamakoshi, D. Finegold, R. Ferrell, D. Kerjaschki, P. Mortimer, S. Ylä-Herttuala, et al. 2004. Defective valves and abnormal mural cell recruitment underlie lymphatic vascular failure in lymphedema distichiasis. *Nat. Med.* 10:974–981. doi:10.1038/nm1094

Podgrabinska, S., P. Braun, P. Velasco, B. Kloos, M.S. Pepper, and M. Skobe. 2002. Molecular characterization of lymphatic endothelial cells. *Proc. Natl. Acad. Sci. USA.* 99:16069–16074. doi:10.1073/pnas.242401399

Ratzinger, G., P. Stoitzner, S. Ebner, M.B. Lutz, G.T. Layton, C. Rainer, R.M. Senior, J.M. Shipley, P. Fritsch, G. Schuler, and N. Romani. 2002. Matrix metalloproteinases 9 and 2 are necessary for the migration of Langerhans cells and dermal dendritic cells from human and murine skin. *J. Immunol.* 168:4361–4371.

Rowe, R.G., and S.J. Weiss. 2008. Breaching the basement membrane: who, when and how? *Trends Cell Biol.* 18:560–574. doi:10.1016/j.tcb.2008.08.007

Sauter, B., D. Foedinger, B. Sterniczky, K. Wolff, and K. Rappersberger. 1998. Immunoelectron microscopic characterization of human dermal lymphatic microvascular endothelial cells. Differential expression of CD31, CD34, and type IV collagen with lymphatic endothelial cells vs blood capillary endothelial cells in normal human skin, lymphangioma, and hemangioma in situ. *J. Histochem. Cytochem.* 46:165–176.

Swartz, M.A. 2001. The physiology of the lymphatic system. *Adv. Drug Deliv. Rev.* 50:3–20. doi:10.1016/S0169-409X(01)00150-8

Teoh, D., L.A. Johnson, T. Hanke, A.J. McMichael, and D.G. Jackson. 2009. Blocking development of a CD8+ T cell response by targeting lymphatic recruitment of APC. *J. Immunol.* 182:2425–2431. doi:10.4049/jimmunol.0803661

Trzewik, J., S.K. Mallipattu, G.M. Artmann, F.A. Delano, and G.W. Schmid-Schönbein. 2001. Evidence for a second valve system in lymphatics: endothelial microvalves. *FASEB J.* 15:1711–1717. doi:10.1096/fj.01-0067com

Vainionpää, N., R. Bützow, M. Hukkanen, D.G. Jackson, T. Pihlajaniemi, L.Y. Sakai, and I. Virtanen. 2007. Basement membrane protein distribution in LYVE-1-immunoreactive lymphatic vessels of normal tissues and ovarian carcinomas. *Cell Tissue Res.* 328:317–328. doi:10.1007/s00441-006-0366-2

Wang, S., M.B. Voisin, K.Y. Larbi, J. Dangerfield, C. Scheiermann, M. Tran, P.H. Maxwell, L. Sorokin, and S. Nourshargh. 2006. Venular basement membranes contain specific matrix protein low expression regions that act as exit points for emigrating neutrophils. *J. Exp. Med.* 203:1519–1532. doi:10.1084/jem.20051210

Wei, S.H., H. Rosen, M.P. Matheu, M.G. Sanna, S.K. Wang, E. Jo, C.H. Wong, I. Parker, and M.D. Cahalan. 2005. Sphingosine 1-phosphate type 1 receptor agonism inhibits transendothelial migration of medullary T cells to lymphatic sinuses. *Nat. Immunol.* 6:1228–1235. doi:10.1038/ni1269

Wolf, K., R. Müller, S. Borgmann, E.B. Bröcker, and P. Friedl. 2003. Amoeboid shape change and contact guidance: T-lymphocyte crawling through fibrillar collagen is independent of matrix remodeling by MMPs and other proteases. *Blood.* 102:3262–3269. doi:10.1182/blood-2002-12-3791

Wolf, K., Y.I. Wu, Y. Liu, J. Geiger, E. Tam, C. Overall, M.S. Stack, and P. Friedl. 2007. Multi-step pericellular proteolysis controls the transition from individual to collective cancer cell invasion. *Nat. Cell Biol.* 9:893–904. doi:10.1038/ncb1616

Wyckoff, J.B., S.E. Pinner, S. Gschmeissner, J.S. Condeelis, and E. Sahai. 2006. ROCK- and myosin-dependent matrix deformation enables protease-independent tumor-cell invasion in vivo. *Curr. Biol.* 16:1515–1523. doi:10.1016/j.cub.2006.05.065